Universidade de São Paulo

Biblioteca Digital da Produção Intelectual - BDPI

Departamento de Física - FFCLRP/591

Artigos e Materiais de Revistas Científicas - FFCLRP/591

2012-04-28

Synthesis and characterization of silver/alanine nanocomposites for radiation detection in medical applications: the influence of particle size on the detection properties

Nanoscale

PAPER

Synthesis and characterization of silver/alanine nanocomposites for radiation detection in medical applications: the influence of particle size on the detection properties

Eder José Guidelli,[*a] **Ana Paula Ramos,**[b] **Maria Elisabete D. Zaniquelli,**[b] **Patricia Nicolucci**[a] **and Oswaldo Baffa**[a]

Silver/alanine nanocomposites with varying mass percentage of silver have been produced. The size of the silver nanoparticles seems to drive the formation of the nanocomposite, yielding a homogeneous dispersion of the silver nanoparticles in the alanine matrix or flocs of silver nanoparticles segregated from the alanine crystals. The alanine crystalline orientation is modified according to the particle size of the silver nanoparticles. Concerning a mass percentage of silver below 0.1%, the nanocomposites are homogeneous, and there is no particle aggregation. As the mass percentage of silver is increased, the system becomes unstable, and there is particle flocculation with subsequent segregation of the alanine crystals. The nanocomposites have been analyzed by transmission electron microscopy (TEM), UV-Vis absorption spectroscopy, X-ray diffraction (XRD), and Fourier transform infrared (FTIR) spectroscopy and they have been tested as radiation detectors by means of electron spin resonance (ESR) spectroscopy in order to detect the paramagnetic centers created by the radiation. In fact, the sensitivity of the radiation detectors is optimized in the case of systems containing small particles (30 nm) that are well dispersed in the alanine matrix. As the agglomeration increases, particle growth (up to 1.5 μm) and segregation diminish the sensitivity. In conclusion, nanostructured materials can be used for optimization of alanine sensitivity, by taking into account the influence of the particles size of the silver nanoparticles on the detection properties of the alanine radiation detectors, thus contributing to the construction of small-sized detectors.

1. Introduction

The size-dependent properties of materials at the nanoscale have attracted the attention of many scientists. These distinct features have allowed for the application of such nanomaterials in physics, chemistry, biology, medicine, and health sciences in general. In particular, metal nanoparticles have been employed in medical diagnosis,[1,2] drug delivery systems,[3] wound healing,[4] treatments based on radiation therapy,[5–8] sensors,[9] and radiation detectors,[10,11] just to name a few applications. For instance, a liquid detector based on Ag nanoparticles has been recently developed for dosimetry purposes.[10] In this case, the intensity of the plasmonic absorption peak has been shown to increase with the absorbed dose in a linear regime.[10] Despite this application, the use of nanoparticles in radiation detectors has a similar function to that of radiation therapy in the case of cancer treatments.[11–15] The metal nanoparticles raise the mass absorption coefficient of the tumor tissues and of the radiation detector, thereby augmenting the absorbed dose.[11–13]

The use of alanine as radiation detectors stems from the fact that the interaction between the ionizing radiation and the alanine molecules produces free radicals.[16] The alanine radical that is stable at room temperature is the alanine molecule depleted of the amine group, which furnishes an unpaired electron at the central carbon atom.[17] Hence, these radiation-induced free radicals can be detected by means of an electron spin resonance (ESR) spectrometer. Owing to the hyperfine interactions of the unpaired electron with four hydrogen atoms in the stable $CH_3CHCOOH$ radical, the typical ESR spectrum of the latter species consists of five lines, whose relative intensities obey a $1 : 4 : 6 : 4 : 1$ ratio.[18] The intensity of the signal is proportional to the amount of free radicals present in the exposed sample, and there is a linear relationship with the incident dose of radiation.[18] Thus, for the sake of radiation detection, the peak-to-peak amplitude of the most intense central line of the ESR spectrum is utilized, being proportional to the concentration of free radicals. However, alanine has its

[a]Departamento de Física, Faculdade de Filosofia, Ciências e Letras de Ribeirão Preto, Universidade de São Paulo, Av. Bandeirantes, 3900, 14040-901 Ribeirão Preto, SP, Brazil. E-mail: ederguidelli@pg.ffclrp. usp.br; Tel: +55 (16) 3602-3857
[b]Departamento de Química, Faculdade de Filosofia, Ciências e Letras de Ribeirão Preto, Universidade de São Paulo, Av. Bandeirantes, 3900, 14040-901 Ribeirão Preto, SP, Brazil

sensitivity reduced in the case of low doses and low-energy photons (energy below 100 keV).[18,19]

The poor sensitivity of low energies and doses, the growing need for cancer treatments that employ radiosurgery and intensity modulated radiation therapy (IMRT) makes the accomplishment of dosimetry of narrow photon beams crucial.[20–23] In this context, the utilization of small radiation detectors is required, in order to obtain enough spatial resolution.[24–27] Because the sensitivity of alanine detectors depends on the amount of free radicals that is produced by the radiation, a reduction in the size of the detector also diminishes its sensitivity.[28]

Fortunately, at the same time that alanine is suitable for use in radiation detectors, it accumulates the functions of reducing, capping, and stabilizing agent for the production of silver nanomaterials. In fact, the preparation of silver nanoparticles using alanine, aiming at the nanocomposites as radiation detectors by means of the ESR technique, has also been recently developed in our laboratory.[10] The nanocomposites display improved sensitivity and diminished energy dependence as compared to pure DL-alanine.[11] The enhancement in the sensitivity of the radiation detection due to the presence of silver nanoparticles, which have a high atomic number, is attributed to the electrons ejected by the metal upon its interaction with the ionizing radiation, thereby delivering the dose to the detecting material.[11,29–31] Increased sensitivity can also be achieved in composites containing material with high atomic number that are not in the nanoscale.[19–21] However, when it comes to the construction of small radiation detectors, it should be borne in mind that inhomogeneities in the composite can significantly reduce the sensitive volume of the detector, thus implying in wrong assessment of the dose.

In this sense, considering that the use of other metal nanoparticles enables enhancement of the delivered dose, it has been reported that the dose deposition in a medium surrounding gold nanoparticles depends on the particles' size.[32] The energy deposition outside the gold nanoparticles as a percentage of the total energy deposition (the dose outside the nanoparticles + self-absorbed dose) decreases as the diameter of the gold nanoparticles increases from 2 up to 100 nm.[32] The percentage of self-absorbed dose for 100 nm gold nanoparticles reaches values greater than 30%.[32]

Recently, computational simulations have been employed to predict the improvement in the sensitivity of Gd_2O_3/alanine composites used as radiation detectors.[33] The simulation setup consisted of 1.5 μm Gd_2O_3 spherical particles homogeneously dispersed in an alanine matrix, and particle overlap (aggregation) was assumed not to occur.[33] However, in real situations, the stability of the particles in a composite is dictated by many physicochemical factors, driving the system toward homogeneity or particle aggregation (particle overlap). This can dramatically modify the dose deposition profile and can consequently alter the detection properties of the detectors.

In this context, the production of metal nanoparticles and their stabilization by biomolecules have been extensively studied.[34–36] At the same time that the morphology and properties of the silver nanoparticles are strongly influenced by the nature of the reducing agent and the pH of the medium,[37] it has also been shown that the amount of a given reducing/capping agent has a marked effect on particle size distribution.[38,39] Although the use of alanine as reducing and capping agent for the production of silver nanoparticles affords samples with better detection properties, we have noticed that an alanine/silver stoichiometry must be obeyed.[11] This limits the quantity of silver nanoparticles in the alanine matrix.

Therefore, an improvement in the radiation detection using silver/alanine nanocomposites demands a systematic study of how the nanoparticles are dispersed in the matrix and of what the influence of the Ag^+/alanine ratio on the final nanocomposites. Moreover, in order to overcome the limitation of the amount of silver that is used in the synthesis of the Ag/alanine nanocomposite, we have employed another reducing agent, and alanine has been employed as the stabilizer of the colloidal dispersion and a matrix for the nanocomposite. Thus, this work investigates the morphological and structural features of nanocomposites with varying amounts of silver nanoparticles, produced by chemical reduction with sodium borohydride,[37] as well as the ability of alanine to stabilize and accommodate the silver nanoparticles in its crystalline matrix. The application of the nanocomposites as radiation detectors has been evaluated with the aid of the ESR technique. The effect of the particle size of the silver nanoparticles, its interaction with the alanine molecules, the aggregation and segregation of particles inside the alanine matrix, and the way the morphology and the state of agglomeration change the detecting properties of the alanine detectors have been analyzed.

2. Materials and methods

2.1 Silver/alanine nanocomposites preparation

The chemicals employed in the experiments were of analytical reagent grade and were used as received. Silver nitrate (99.8%) was provided by Cennabras, sodium borohydride was purchased from Sigma, and DL-alanine (99%) was obtained from Acros Organics. All the aqueous solutions were prepared with purified Milli-Q™ water. Silver nanoparticles were produced by means of the chemical reduction of silver nitrate.[37] To this end, a 2 mmol L^{-1} $AgNO_3$ aqueous solution was added to a freshly prepared 4 mmol L^{-1} $NaBH_4$ aqueous solution. The color of the system became immediately bright yellow, indicating the formation of a colloidal dispersion. To ensure the total reduction of the silver ions, the system was kept under vigorous stirring for 12 hours. UV-Vis spectroscopy confirmed the formation of silver nanoparticles as seen from the plasmonic absorption peak at 390 nm. The average sizes of the silver nanoparticles present in the freshly prepared colloidal dispersion were estimated by the dynamic light scattering (DLS) technique, which gave a mean size of 30 nm. The stability of these sols was good and there was no breaking down of the colloid within a period of 3 weeks. Therefore, DL-alanine, the matrix of the nanocomposite, was used also as a dispersant in different proportions (Table 1), by addition of different volumes of the colloidal silver dispersion to a 1.1 mol L^{-1} aqueous solution of this amino acid. The mass percentage of silver in the nanocomposites was varied from 0.01% up to 10%. The water was evaporated from the samples in an oven at a temperature of 40 °C, to yield the powdered nanocomposites. The samples were labeled according to the mass

Table 1 Mass percentage of the components present in each sample and its respective sample name

DL-Alanine (% mass)	NpAg (% mass)	Sample name
100.0	0.00	0%NpAg
99.99	0.01	0.01%NpAg
99.98	0.02	0.02%NpAg
99.975	0.03	0.025%NpAg
99.95	0.05	0.05%NpAg
99.90	0.10	0.1%NpAg
99.50	0.50	0.5%NpAg
99.00	1.00	1%NpAg
97.00	3.00	3%NpAg
95.00	5.00	5%NpAg
90.00	10.0	10%NpAg

percentage of silver present in the dried nanocomposites, as it can be seen from Table 1. For example, the nanocomposite prepared with Ag+ 0.01% w/w was named 0.01%NpAg, and so on, up to the sample 10%NpAg.

2.2 Characterization techniques

An Ultrospec 2100 pro (Amersham Pharmacia) spectrophotometer was employed for registration of the UV-Vis absorption spectra of the colloidal dispersions. The average particle size was obtained by the dynamic light scattering (DLS) technique, with the aid of a Zeta-Sizer system (Malvern Instruments), at a fixed wavelength (633 nm He–Ne laser) and angle (90°). The X-ray diffraction (XRD) patterns of the powdered nanocomposites were acquired on a SIEMENS D5005 diffractometer, over the range $20° \leq 2\theta \leq 80°$, with an increment of 0.02°. The CuKα emission line (1.541 Å, 40 kV, 40 mA) coupled to a graphite monochromator was used. The morphology and size of the nanocomposites were investigated on a JEOL-JEM-100 CXII transmission electron microscope (TEM), by drying a drop of the colloidal dispersions on a copper grid covered with a conductive polymer. The Fourier-transform infrared (FTIR) spectra were recorded on a Bomem MB 100 spectrometer, in the region between 4000 and 40 cm^{-1}, using the KBr pellet technique. All these experiments were performed at room temperature.

2.3 Irradiation of samples

The aim of this work was the investigation of the influence of silver nanoparticles on the structural and dosimetric properties of the nanocomposites. Once the influence of high atomic number materials is more relevant for low energy photons, the powdered nanocomposites were irradiated on a Siemens Stabilipan II clinical orthovoltage. To this end, the nanocomposites (~30 mg) were placed into capsules with dimensions of 1.0 × 0.5 cm. Thereafter, the capsules were placed over a 10 cm acrylic layer phantom, in order to avoid particle scattering. Due to the distance of the X-ray source to the sample no build-up cap was utilized. The samples were irradiated with a dose of 5 Gy to furnish a good signal to noise ratio. The kVp was 180 kV, and a 1.28 mmCu filter was employed. The effective energy of the X-ray beam was 90 keV, as calculated by the half value layer (HVL). A 40 cm source-to-dosimeter distance was used, and the field size was 8 × 10 cm^2. These irradiations were carried out at the Radiotherapy Service of HC-FMRP-USP.

In order to cover the total dose range from 1 up to 50 Gy and plot the dose–response curve, the samples were irradiated at the Department of Physics—FFCLRP-USP. The X-ray source was an industrial X-ray tube (Philips, PW 2215/20) with a stationary molybdenum (Mo) target, adapted with a filter of Al, and attached to a constant-potential generator (Philips PANalytical, PW 3830). The tube operates at 35 kVp and 30 mA. The X-ray spectrum was published elsewhere.[40] These irradiations were performed in air, with a source-to-dosimeter distance of 50 cm.

2.4 ESR measurements

ESR spectra of the irradiated powdered nanocomposites were obtained on a JEOL-JES-FA 200 (9.5 GHz) ESR spectrometer. Approximately 30 mg of the powder was placed into a quartz tube positioned in the center of the standard JEOL cylindrical cavity, to ensure that all the samples were within the active volume of the ESR cavity.

The radical produced in the samples containing nanoparticles is the same as that obtained in the case of pure DL-alanine,[11] so the same ESR parameters were employed for the measurements, as follows: room temperature, microwave power = 5 mW, central field at 338.5 mT, sweep width of 10 mT, sweep time of 1 min, modulation amplitude of 0.4 mT, gain of 3000×, and time constant of 0.3 s. An averaging of 5 scans (sweeps) was performed for each sample.

Each spectrum was normalized by the total mass of its respective sample, *i.e.*, mass of alanine + mass of silver nanoparticles, for comparison of the signal amplitudes of the different nanocomposites.

2.5 Theoretical and experimental determination of the dose enhancement factor

The increased sensitivity (gain) observed in the case of nanocomposites applied as radiation detectors is proportional to the rise in the dose delivered to the alanine molecules, due to the presence of nanoparticles with high atomic number, because alanine presents a linear relationship with the dose in the studied dose range (1–50 Gy). This gain in sensitivity for the nanocomposites, or the dose enhancement factor (DEF), can be theoretically predicted as the ratio between the mass absorption coefficient of the nanocomposites by the mass absorption coefficient of pure alanine,[11] as follows:

$$\mathrm{DEF} \approx \frac{(\mu_{\mathrm{en}}/\rho)_{\mathrm{Nc},h\nu}}{(\mu_{\mathrm{en}}/\rho)_{\mathrm{ala},h\nu}} \quad (1)$$

where $(\mu_{\mathrm{en}}/\mu)_{h\nu}$ is the radiation mass absorption coefficient for photons with an specific energy, $h\nu$; the subscripts Nc and ala account for nanocomposite and pure alanine, respectively. The expected mass absorption coefficients for the ionizing radiation were obtained from the National Institute of Standards and Technology—NIST, "Physical Reference Data"[41] database.

Experimentally, the DEFs were calculated as the quotient of the peak-to-peak amplitude of the central line of the ESR spectra obtained for the irradiated nanocomposites and pure alanine. Here it is worth noting that the theoretical prediction assumes that the samples are exposed to a monochromatic X-ray beam. However, a polychromatic X-ray beam with an effective energy

of 90 keV was used for the experiments, as described above. So the effective energy of the beam was employed for the theoretical calculations. Although the effective energy of the beam does not provide the exact value of DEF (since it does not consider the spectral distribution of photon energies of the X-ray beam), it can be used to predict the behavior of the DEF as a function of the mass percentage of silver in the nanocomposites, as will be discussed later.

3. Results and discussion

The UV-Vis spectra obtained for all the samples are depicted in Fig. 1. All the colloidal dispersions display an absorption peak at 390 nm, characteristic of spherical silver nanoparticles.[42] This absorption peak is related to the collective oscillation of the free conducting electrons at the surface of the metal nanoparticles, also known as the surface plasmon resonance band.[42] The position of the peak refers to the size of the particles, and the full width at half maximum (FWHM) is associated with the size distribution of the nanoparticles.[43] It is possible to note a second absorption peak for samples containing a mass percentage of silver higher than 0.05%. As the mass percentage of silver increases, the second absorption peak becomes more intense. For the sample 1%NpAg, this peak is as intense as the absorption peak at 390 nm. For higher mass percentage of silver, the intensity of the peak around 600 nm decreases while its FWHM increases.

The presence of two absorption bands in the UV-Vis spectra suggests particle agglomeration and/or even the formation of nanorods in solution,[44–46] since in an elongated particle the free electrons can oscillate along the particle in the longitudinal and transversal axis.[44–46] In this case, the band localized at longer wavelengths is attributed to oscillation of the electrons along the longitudinal axis and the other one is assigned to the oscillation of the free electrons along the transversal axes.[44–46] Thus, the spectra indicate that the silver nanoparticles undergo morphological changes after interaction with the alanine molecules. For samples with large excess of alanine molecules, i.e., samples 0.01%NpAg, 0.02%NpAg, and 0.025%NpAg, the colloids are stable over a year, and just one absorption peak is observed. In
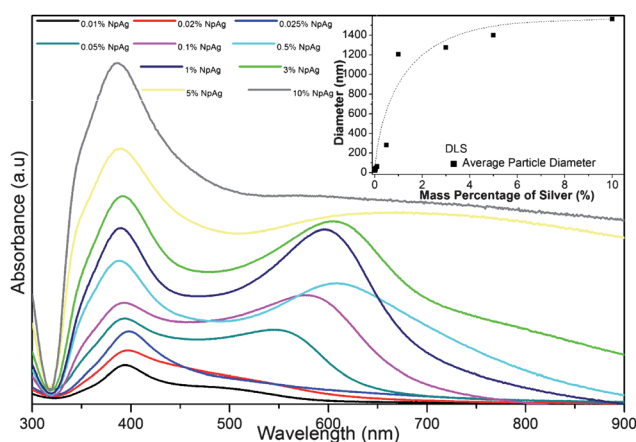
these cases, it is probable that alanine should act as a good stabilizer, thereby avoiding the agglomeration of the particles. As the mass percentage of silver in the system increases, it is also possible to realize that the position of the longitudinal absorption peaks shifts to the red, suggesting an increase in size of the nanoparticles.[45] For the samples 5%NpAg and 10%NpAg, the second absorption peak becomes less intense with concomitant rise in the FWHM, indicating the higher state of aggregation of the system. The size of the particles measured by the dynamic light scattering technique confirms these observations (inset of Fig. 1). For samples containing from 0.01% up to 0.1% silver, the average particle size is 30 nm. As for the sample 0.5%NpAg, the average particle size is 280 nm. Concerning samples from 1% NpAg up to 10%NpAg particles larger than 1 μm can be detected.

Computational simulations have revealed that morphological changes of solid particles in a binary liquid mixture occur due to strong attractive interactions among particles when the total volume of the more wettable phase is not enough to cover all the particles.[47,48] On the basis of these results it can be assumed that the number of alanine molecules is not enough to stabilize the system against flocculation in the presence of larger concentrations of silver nanoparticles, thereby causing the aggregation and modifying the shape of the particles,[47,48] as discussed above. Thus, the increase in particle size and the morphological changes, evidenced by the UV-Vis spectra and the DLS results, reduce the surface area of the nanoparticles as the number of alanine molecules per particle decreases.

The diffractograms obtained from the powders of the samples 0.01%NpAg, 0.1%NpAg, 0.5%NpAg and 1%NpAg are presented in Fig. 2(a). The silver nanoparticles have a crystalline structure with face-centered cubic phase, attributed to the presence of peaks related to planes with Miller indices of (111), (200), (311), and (222).[49,50] From the diffractograms it is also possible to estimate the size of the nanoparticles by means of the Debye–Scherer equation. This equation gives an approximation for the medium size of nanocrystallites on the basis of the FWHM of the peaks of the diffractograms. Table 2 shows the FWHM of the peak related to the plane (111), which is the most intense of the crystalline structure of silver. It is possible to note that as the mass percentage of silver in the nanocomposite increases, the FWHM decreases. Once the FWHM is inversely proportional to the size of the particles, it can be inferred that there is an increase in the mean diameter of the silver nanoparticles as the mass percentage of silver nanoparticles is raised, which is the same trend obtained by means of DLS and UV-Vis spectra. However, because the UV-Vis spectra have also evidenced alterations in particle morphology, the diameter of particles could not be calculated by means of the Debye–Scherer equation because it considers a geometric parameter that depends on the shape of the particle.

The diffraction peaks sitting at 20.7°, 29.7°, 30.8°, 33.2°, and 34.9° are ascribed to DL-alanine,[51] corresponding to the planes with (210), (400), (002), (410), and (112) Miller indices, respectively. These peaks confirm the orthorhombic crystalline structure of DL-alanine. However, the intensity ratios for the peaks at 29.7° and 30.8° depend on the Ag+/alanine ratio. In the case of the sample 0%NpAg the peak at 29.7° is more intense than the peak at 30.8°, whereas for the sample 0.01%NpAg the peak
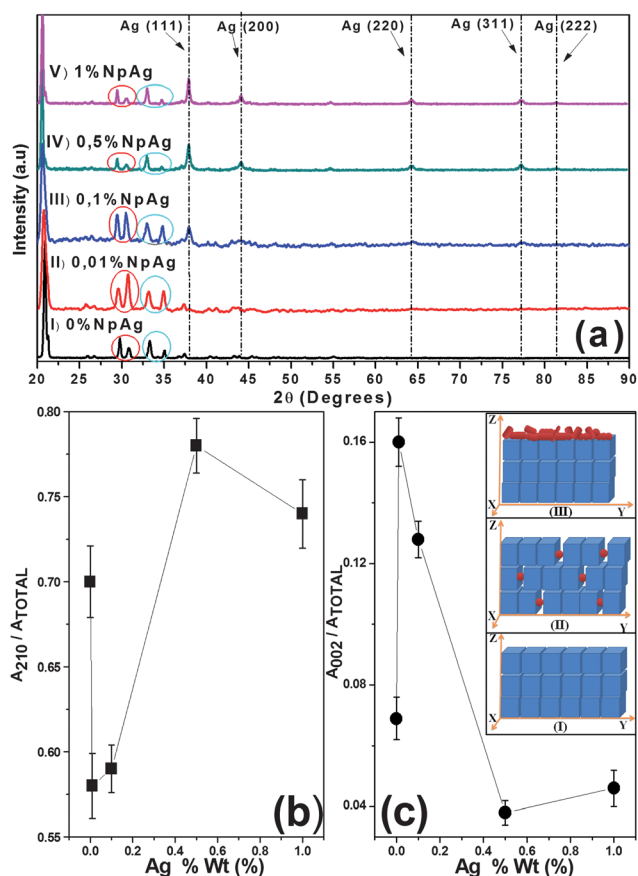

Fig. 1 UV-Vis spectra of the silver nanoparticles. The inset corresponds to the averaged particle size obtained by the dynamic light scattering technique.

Fig. 2 (a) XRD pattern of the nanocomposites. Crystallinity of the (b) (210) and (c) (002) planes of DL-alanine. The crystallinity was measured as the area of each peak in the XRD pattern of DL-alanine divided by the total area of the peaks associated with the orthorhombic crystalline structure of DL-alanine.

Table 2 FWHM of the peak related to the (111) plane of the fcc structure of the silver nanoparticles, for samples with different mass percentages of silver

Sample	FWHM
0.01%NpAg	0.81
0.1%NpAg	0.51
0.5%NpAg	0.40
1%NpAg	0.31

intensities are inverted, and for the sample 0.1%NpAg the peak intensities are equal. These peaks are marked with red circles in Fig. 2(a). A similar behavior can be noted for the peaks at 33.2° and 34.9°, as highlighted with blue circles in the same figure. Hence, the insertion of a small amount of silver nanoparticles in an alanine matrix seems to favor the crystalline orientation of the organic molecule along the planes (002) and (112). When it comes to the samples 0.5%NpAg and 1%NpAg, the peaks at 29.7° and 33.2° are more intense as compared to the peaks at 30.8° and 34.9°, respectively, suggesting that in the case of samples with larger quantity of silver nanoparticles, alanine crystallizes in a similar way as compared to alanine in the case of absence of such nanoparticles.

The crystallinity of alanine can be estimated by dividing the area of each peak by the total area of the peaks associated with the orthorhombic crystalline structure of DL-alanine. Fig. 2(b) displays the crystallinity of alanine measured by means of the (210) plane as a function of the mass percentage of silver. The (210) crystallinity diminishes from 70% in the case of sample 0% NpAg to 58% for the samples 0.01%NpAg and 0.1%NpAg. Thereafter, it increases up to 78% for the samples 0.5%NpAg and 1%NpAg. In contrast, the crystallinity of alanine measured on the basis of the (002) plane rises from 7% in the case of sample 0% NpAg up to 16% for the sample 0.01%NpAg and decreases to 5% for the sample 1%NpAg (Fig. 2(c)).

These results indicate that the silver nanoparticles affect the crystallization of alanine. As described in the literature, the alanine molecules can form amorphous nanoparticles, which crystallize and give rise to mesocrystals that thereafter furnish alanine single crystals.[51–53] On the other hand, there are literature works stating that the presence of nanoparticles can modify the molecular orientation, the crystallization temperature, the crystallization degree, and the crystallization rate of the matrix of a nanocomposite.[54,55] Indeed, it has been reported that gold nanoparticles favor the crystalline orientation of L-alanine crystals preferentially along the c-axes.[56] On the basis of these observations, the scheme shown as inset (I) in Fig. 2(c) hypothetically illustrates the ordered crystal growth of alanine, preferentially along the Y-axis. By adding a low amount of silver nanoparticles, the latter would be accommodated inside the alanine crystals, thereby causing disorder of the crystallites, and favoring the crystalline orientation along the (002) plane at the expense of the (210) plane. This situation is represented in Fig. 2(c), inset (II). By raising the quantity of silver nanoparticles, the colloids become unstable, giving rise to particle agglomeration, morphological alterations and enlarged particles size, as evidenced by the UV-Vis, DLS, and XRD results. This particle growth would preclude the insertion of particles inside the alanine crystalline structure. In this way, the large particles segregate from alanine, which can crystallize without defects in its structure, as illustrated in Fig. 2(c), inset (III). Thus, the growth of alanine crystal seems to depend on the sizes and/or shape of the silver nanoparticles as a consequence of the position of these particles in the alanine matrix.

Similar results have been reported in the case of polymer/nanoparticle composites. By means of computational simulations it has been demonstrated that small particles are dispersed in a microdomain, whereas large particles localize at the center of that microdomain.[48,57] This occurs because, during the formation of the polymeric chain, the polymer must stretch around the solid nanoparticles, which causes loss of system entropy. This loss depends on the size of the particles, and it increases as the diameter of the nanoparticles augments.[48,57] In this sense, the spatial distribution of nanoparticles in a polymeric microdomain can be adjusted according to the nanoparticles size relative to the radius of gyration of the polymer.[48,58] It has been also revealed that in the absence of interaction between the polymer and the nanoparticles, the smaller particles are still dispersed, whilst the larger particles are totally expelled from the polymeric matrix.[48,57] These results reinforce the hypothesis that for samples containing a low amount of silver nanoparticles, the small size of the particles (30 nm) produces good dispersion of
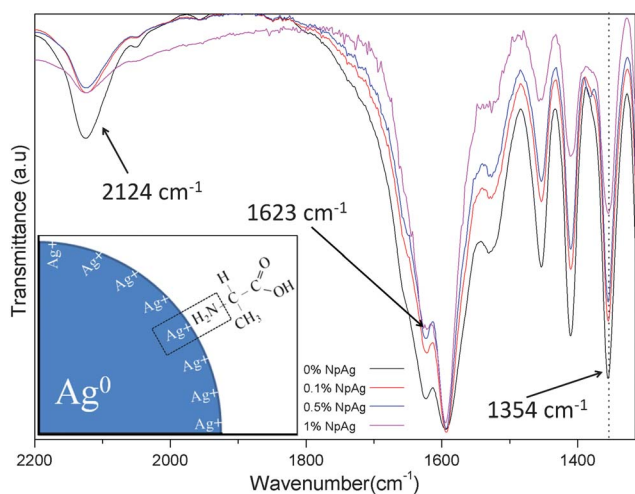
Fig. 3 FTIR spectra of the non-irradiated samples of pure DL-alanine and for silver/alanine nanocomposites.

the nanoparticles inside the alanine matrix. The rise in the concentration of silver nanoparticles causes growth of the particles (up to 1.5 μm) as well as morphological changes, leading to the particles being expelled from the alanine crystals.

Fig. 3 shows the FTIR spectra of the non-irradiated samples 0%NpAg, 0.1%NpAg, 0.5%NpAg, and 1%NpAg. The vibrational spectra of DL-alanine are consistent with the characteristic FTIR spectrum of alanine.[59,60] Taking the band corresponding to the C–H deformation at 1354 cm^{-1} as an internal standard, the relative intensity of the bands $I_{(C-H)}/I_{(N-H)}$ reveals the reduction of the vibration bands associated with the –NH$_3$ groups. The C–H deformation band has been selected for analysis because formation of complexes between silver ions and –CH$_3$ radicals is not known from the literature. The largest variations can be observed for the symmetric and asymmetric stretching of the N–H bond at 2124 and 1623 cm^{-1}. The relative intensity of the

band at 2124 cm^{-1} decreases by about 30% as compared to the same band in the spectrum of pure DL-alanine. The band at 1623 diminishes about 17%.

Some authors have reported that the formation of an alanine–copper complex causes disappearance of the vibration band around 2100 cm^{-1}.[61] This suggests that the silver nanoparticles may interact with the amine group of the DL-alanine molecules, thereby reducing the relative intensities of the vibrational bands of the N–H bond, as observed above. Furthermore, the amine groups of L-alanine have been found to interact onto silver nanostructures, acting as nucleation sites for crystal growth.[62] The amine groups also play a role in the reduction of silver ions during the synthesis of nanoparticles.[11,63] Thus, our data indicate that the stabilization of the silver nanoparticles is mainly due to an interaction of the silver ions adsorbed onto the surface of the nanoparticles with the amine group of the DL-alanine molecules.

Fig. 4 displays the TEM micrographs obtained for the analyzed samples. Fig. 4(a) shows the TEM images of the sample 0.01%NpAg. The particles are spherical and well dispersed, as suggested by the UV-Vis spectroscopy. Fig. 4(b) and (c) correspond to samples 1%NpAg and 3%NpAg. Both pictures evidence the agglomeration, the growth and the formation of elongated particles, confirming the predictions from the UV-Vis results. The elongated particles seem to be formed by the linear assembly of spherical particles, as depicted in Fig. 4(c). Thus, the TEM images endorse the hypothesis that the aggregation, growth, and morphological changes occur in an attempt to reduce the total area of nanoparticle surface, as the number of alanine molecules per particle is lowered.

Fig. 4(d)–(f) are related to the samples 3%NpAg and 5%NpAg. These images have been recorded with reduced magnification. Due to the high electronic density of silver, it is possible to distinguish the silver particles from the alanine matrix. The arrow in Fig. 4(c) points to a region where the silver particles are accommodated outside the alanine matrix. Fig. 4(d) and (f) illustrate the formation of nanostructured agglomerates, which
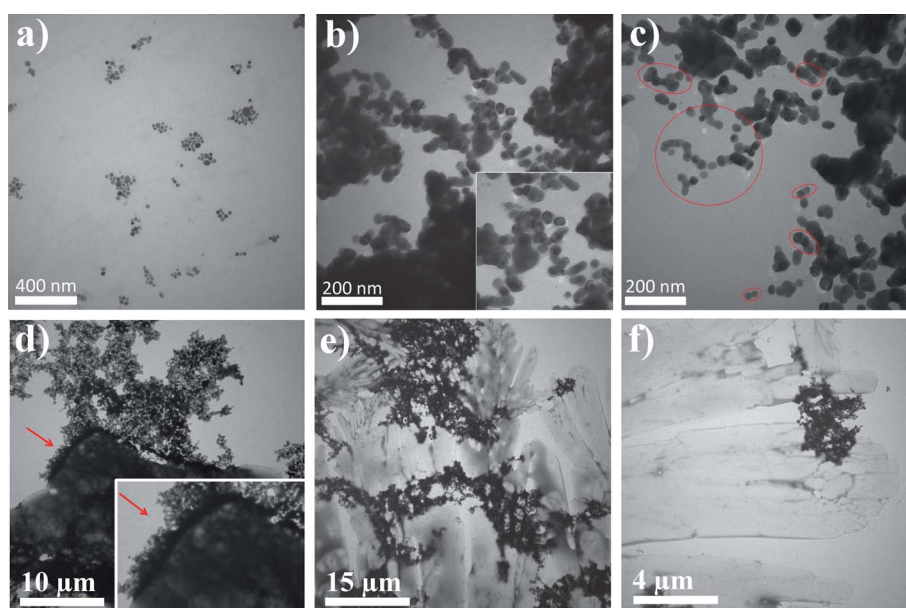

Fig. 4 TEM micrographs of the silver/alanine nanocomposites: (a) 0.01%NpAg; (b) 3%NpAg; (c) 1%NpAg; (d) 3%NpAg; (e) and (f) 5%NpAg.

clearly seem to be segregated from the alanine matrix. Thus, the TEM images corroborate the assumption that the agglomerates are expelled from the alanine matrix, so that the nanocomposites with high mass percentage of silver are composed of segregated silver particles.

The segregation of nanoparticles has also been described for nanocomposites of polystyrene containing CdSe nanoparticles. In this case, the nanoparticles segregate at the cracks existing in the polymer film.[48,64] It has also been reported that gold nanoparticles are preferentially located at the interface between polystyrene and poly(styrene-b-2-vinylpyridine) composites.[48,65] In another system containing CdSe nanoparticles dispersed on poly(methyl methacrylate), it was observed that the largest nanoparticles were localized at the film cracks, whereas the smallest one was accommodated in the polymeric matrix with no great alteration in the system entropy.[48,66] These changes in the system entropy increase as the size of the nanoparticles augments.[48,57] Our group has also detected that larger silver nanoparticles (40 nm) are produced by the diffusion of the small nanoparticles (2 nm) to the edge of latex films, causing an increase in the size of the particles due to aggregation.[34] Hence, the growth of the particles and formation of nanostructured agglomerates of silver seem to result in the expulsion of the nanoparticles from the alanine matrix, thus culminating aggregation and segregation of the particles outside the alanine crystals, as verified by the XRD patterns and in TEM micrographs.

The samples have been employed as radiation detectors using the ESR technique. Fig. 5(a) shows the ESR spectra of the samples 0%NpAg and 10%NpAg irradiated with an X-ray beam with effective energy of 90 keV. This is the characteristic spectrum of the stable $CH_3CHCOOH$ radical stemming from the exposure of alanine to ionizing radiation.[67] The increased peak-to-peak amplitude (A_{pp}) of the central line of the spectrum of the sample 10%NpAg evidences the improved sensitivity of the samples containing silver nanoparticles. This enhancement is attributed to the increased interaction of the X-ray photons with the metal nanoparticles, giving rise to photoelectrons that effectively deliver dose to the alanine molecules around the nanoparticles, thus elevating the production of free radicals.[11,30,31] This is one advantage of using alanine as the capping agent instead of any other passivating molecule.

On the basis of the theoretical prediction, it should be expected that upon raising the amount of silver nanoparticles in the alanine matrix there would be an increase in the sensitivity of alanine, due to the larger mass absorption coefficient of the samples.[11,13] The inset in Fig. 5(b) shows that the theoretical prediction also establishes a linear relationship between the gain in sensitivity (or dose enhancement factor—DEF) and the mass percentage of silver. Other authors have also reported this linear behavior of the DEF with Gd_2O_3 concentration by means of a computational simulation.[33] Nevertheless, our experimental results demonstrate that this relationship is nonlinear, as shown in Fig. 5(b). For the samples 0.01%NpAg and 0.1%NpAg, the DEF is 1.46 ± 0.16 and 1.58 ± 0.12, respectively; i.e., the sensitivity rises to 46 and 58% as compared to that of pure alanine (0%NpAg). However, for the sample 0.5%NpAg the DEF decreases to 1.53 ± 0.09, reaching a minimum value of 1.30 ± 0.08 for the sample 1%NpAg.

Here it is noteworthy that the values of the experimental DEFs are always higher than the theoretical DEF, probably because the latter is calculated by using the effective energy of the beam. Since the mass absorption coefficients are higher for lower photon energies, the higher values of the experimental results are most likely due to the contribution of the photons with energy below the effective energy of the beam. Therefore, it is important to emphasize that although the theoretical DEF does not furnish the exact value of DEF, it can be used to show that, theoretically, the DEF increases as the Ag+/alanine ratio rises.

At this point, one may wonder why the sample 1%NpAg has a lower DEF as compared to the sample 0.01%NpAg. According to the theoretical predictions,[11,13] sample 1%NpAg should present greater DEF than sample 0.01%NpAg[11,13,33] (inset of
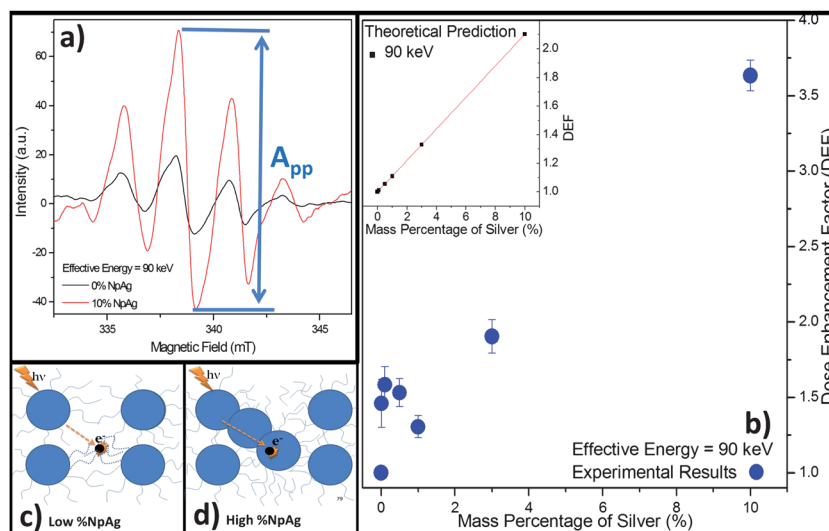

Fig. 5 (a) ESR spectra of the irradiated samples of pure DL-alanine and for the sample 10%NpAg. (b) DEF as a function of the mass percentage of silver in the nanocomposites. The inset corresponds to the theoretical predictions about the DEF. (c) and (d) illustrate the interaction of the electrons ejected by the silver nanoparticles.

Fig. 5(b)). This behavior could be attributed to the structural and morphological alterations taking place in the nanocomposites due to the augmented mass percentage of silver, as pointed by the UV-Vis spectroscopy, DLS, XRD and TEM. The sample 0.01% NpAg presents a UV-Vis spectrum characteristic of spherical silver nanoparticles, with no evidence of aggregation. The particle diameter is 30 nm. The XRD, DLS and TEM techniques have confirmed that the particles are stable in terms of size. The diffractograms have also revealed that the nanoparticles are accommodated inside the crystalline alanine matrix. Therefore, the presence of small non-aggregated spherical particles (30 nm) homogeneously distributed inside the alanine matrix seems to optimize the conditions for the dose deposition in the alanine molecules, thus optimizing the DEF and consequently the sensitivity of alanine when it is used as the radiation detector. Upon rising the mass percentage of silver up to 1% in the nanocomposites (1%NpAg), there is particle agglomeration, morphological changes and particle segregation outside the alanine matrix, and particles larger than 1 μm can be noticed. All the alterations seem to be responsible for the reduction in DEF, although there is an increase in the radiation mass absorption coefficient of the nanocomposites.

For the samples with a small amount of silver nanoparticles (0.01%NpAg up to 0.1%NpAg), the alanine molecules appear to act as a capping agent against particle agglomeration. As a consequence, the nanoparticles become stable and, when the samples are dried, the nanoparticles remain inserted inside the alanine matrix. When these samples containing silver nanoparticles well distributed inside the alanine matrix are employed as radiation detectors, the electron ejected from a given nanoparticle will deliver most of the dose to the alanine molecules in the vicinity of that particle (Fig. 5(c)). This causes the optimization of the DEF and the sensitivity of the nanocomposites. As the mass percentage of silver is increased, the particles agglomerate and grow (up to 1.5 μm), so they are expelled from the alanine matrix, and probably localize on the surface of the crystals, as previously discussed. Thus, in these cases, the electrons ejected from a nanoparticle will deposit most of the dose in the nanoparticles that are in the vicinity, instead of depositing the dose in the alanine molecules (Fig. 5(d)). Since alanine is the molecule responsible for the detection of radiation, the electron which delivers the dose to other nanoparticles does not generate any free radicals, so there is contribution to DEF or to the sensitivity of the nanocomposites. The part of the dose that is absorbed by the metal nanoparticles is the so-called self-absorbed dose.[32] By means of Monte Carlo simulation, it has recently been shown that the self-absorption of radiation by gold nanoparticles in a tissue-equivalent medium augments as the particle size increases.[32] This corroborates the results presented in this paper, suggesting that the size and state of aggregation of particles can alter the response of the detector by increasing/decreasing the self-absorption of the dose by the silver nanoparticles.

Therefore, the gain in sensitivity of the nanocomposites seems to be simultaneously dictated by two factors: the mass percentage of silver in the nanocomposites and the size of the silver nanoparticles. The mass percentage of silver is responsible for increasing the radiation mass absorption coefficient of the composites, thus augmenting the interaction of the radiation with the detector. The size of the particles appears to affect the positioning of the nanoparticles in the alanine matrix and the deposition of dose in the alanine molecules as follows: smaller particles (≈ 30 nm) are accommodated inside the alanine matrix, so the electron ejected from a nanoparticles deliver most of the doses to the alanine molecules in its vicinity, optimizing the DEF. On the other hand, larger particles are expelled to the crystal surfaces. Therefore, the electron ejected from a nanoparticle delivers most of the dose to the silver nanoparticles around it, lowering the DEF. The final response of the detector is given by a balance between the increased mass absorption coefficient due to the addition of the silver nanoparticles, and the dose self-absorbed by the nanoparticles. Indeed, the real dose enhancement factor must account for the portion of dose that is self-absorbed by the nanoparticles. Thus, the mass percentage of silver affects the component related to the ratio of the radiation mass absorption coefficients, whereas the size of the particles influences the self-absorbed dose component.

As discussed before, for a mass percentage of silver smaller than 0.5%, the small-sized particles (30 nm) and the low state of agglomeration optimize the DEF. By augmenting the amount of silver from 0.5% up to 1%, the theoretically expected value of DEF is increased by only 5% (inset of Fig. 5(b)). However, this elevation in the mass percentage of silver causes an increase in the state of agglomeration and in the size of the particles (up to 1.5 μm), as pointed by the previous characterization techniques. Thus, while the rise in the mass absorption coefficient is not so significant, the presence of agglomerates and larger particles is believed to markedly increase the contribution from self-absorption.[32] That is the reason why the experimental DEF drops from 1.53 ± 0.09 down to 1.30 ± 0.08 for the samples 0.5% NpAg and 1%NpAg, respectively. On the other hand, by raising the mass percentage of silver from 1% up to 3%, and from 3% up to 10% the theoretical DEF increases to 22% (inset of Fig. 5(b)) and 80%, respectively. This makes the contribution of the self-absorption in the response of samples 3%NpAg and 10%NpAg less noticeable, giving rise to a DEF of 1.90 ± 0.11 and 3.63 ± 0.1, respectively. Therefore, for a mass percentage of silver larger than 1%, the larger particles cause the DEFs to increase linearly, but below the optimized condition that is obtained in the case of nanocomposites with low Ag$^+$/alanine percentage, which have nanosized particles.
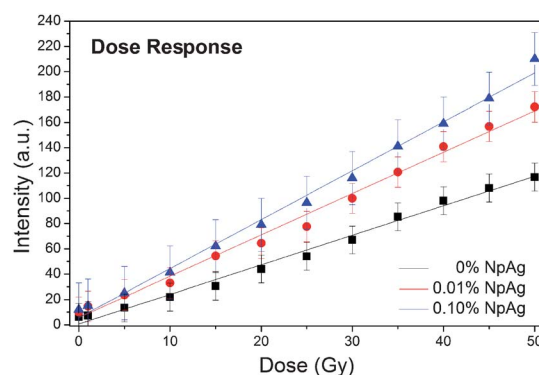

Fig. 6 ESR signal intensity *versus* dose. Signal intensity is proportional to spin concentration per mass and it is given in arbitrary units (a.u.).

The dose–response curves of samples 0%NpAg, 0.01%NpAg, and 0.1%NpAg are shown in Fig. 6. It can be seen that the curves remain linear even after the addition of silver nanoparticles. The slope of the curves are (2.3 ± 0.1) spins (a.u.)/Gy, (3.3 ± 0.1) spins (a.u.)/Gy and (3.9 ± 0.2) spins (a.u.)/Gy respectively. The curves related to samples with a mass percentage of silver above 0.1% are not presented here because some of them override each other, thereby confounding the visualization of the data. However, the slope of their curves are (4.6 ± 0.1) spins (a.u.)/Gy, (3.9 ± 0.2) spins (a.u.)/Gy, (6.9 ± 0.3) spins (a.u.)/Gy, and (8.5 ± 0.2) spins (a.u.)/Gy respectively for the samples 0.5%NpAg, 1% NpAg, 3%NpAg, and 10%NpAg. Thus, it can be concluded that nanomaterials can be used to optimize the sensitivity of alanine radiation detectors.

4. Conclusion

Silver/alanine nanocomposites containing different mass percentage of silver have been synthesized. For low mass percentage of silver, the system is homogeneous, no aggregation is observed, and the nanoparticles are accommodated inside the alanine matrix. As the amount of silver nanoparticles is increased, the system becomes unstable and aggregated, causing morphological changes and the growth of particles. This causes expulsion of the agglomerated particles from the alanine matrix, and segregation outside of the alanine crystals. The silver nanoparticles also influence the alanine crystallization process. The interaction of the silver nanoparticles with alanine occurs *via* the NH groups of the alanine molecules. The nanocomposites display enhanced sensitivity in terms of radiation detection as compared to pure DL-alanine. In fact, the DEF is optimized in a homogeneous system containing small nanoparticles (30 nm), yielding a value higher than that expected for a linear behavior. As the mass percentage of silver is augmented, the aggregation, growth and segregation of the particles elevate the dose that is self-absorbed by the silver nanoparticles, diminishing the DEF, whereas the theoretical prediction points toward enlargement of the DEF. Thus, it is evident that nanostructured materials can optimize the sensitivity of radiation detectors, being potentially useful for miniaturized devices.

Acknowledgements

References

1 L. A. Austin, B. Kang, C.-W. Yen and M. A. El-Sayed, *J. Am. Chem. Soc.*, 2011, **133**, 17594.
2 H. Liu, X. Zhang, B. Xing, P. Han, S. S. Gambhir and Z. Cheng, *Small*, 2010, **6**, 1087.
3 G. Aliev, H. H. Palacios, V. B. Shadlinski, D. Gokhman, K. Gasiorowski and J. Leszek, *European Journal of Neurology*, 2011, **18**, 344.
4 K. H. Kwan, X. Liu and K. W. Yeung, *Nanomedicine*, 2011, **6**, 595.
5 T. Kong, J. Zeng, X. Wang, X. Yang, J. Yang, S. McQuarrie, A. McEwan, W. Roa, J. Chen and J. Z. Xing, *Small*, 2008, **4**, 1537.
6 J. D. Carter, N. N. Cheng, Y. Qu, G. D. Suarez and T. Guo, *J. Phys. Chem. B*, 2007, **111**, 11622.
7 E. Brun, L. Sanche and C. Sicard-Roselli, *Colloids Surf., B*, 2009, **72**, 128.
8 S. J. McMahon, W. B. Hyland, E. Brun, K. T. Butterworth, J. A. Coulter, T. Douki, D. G. Hirst, S. Jain, A. P. Kavanagh, Z. Krpetic, M. H. Mendenhall, M. F. Muir, K. M. Prise, H. Requardt, L. Sanche, G. Schettino, F. J. Currell and C. Sicard-Roselli, *J. Phys. Chem. C*, 2011, **115**, 20160.
9 O. Stranik, H. M. McEvoy, C. McDonagh and B. D. MacCraith, *Sens. Actuators, B*, 2005, **107**, 148.
10 M. Funaro, A. Di Bartolomeo, P. Pelosi, M. S. Saponetti and A. Proto, *Micro Nano Lett.*, 2011, **6**, 759.
11 E. J. Guidelli, A. P. Ramos, M. E. D. Zaniquelli, P. Nicolucci and O. Baffa, *Radiat. Phys. Chem.*, 2011, 301.
12 A. K. Pradhan, S. N. Nahar, M. Montenegro, Y. Yu, H. L. Zhang, C. Sur, M. Mrozik and R. M. Pitzer, *J. Phys. Chem. A*, 2009, **113**, 12356.
13 S. Corde, A. Joubert, J. F. Adam, A. M. Charvet, J. F. Le Bas, F. Esteve, H. Elleaume and J. Balosso, *Br. J. Cancer*, 2004, **91**, 544.
14 C. Minelli, S. B. Lowe and M. M. Stevens, *Small*, 2010, **6**, 2336.
15 G. Le Duc, I. Miladi, C. Alric, P. Mowat, E. Braüer-Krisch, A. Bouchet, E. Khalil, C. Billotey, M. Janier, F. Lux, T. Epicier, P. Perriat, S. Roux and O. Tillement, *ACS Nano*, 2011, **5**, 9566.
16 W. W. Bradshaw, D. G. Cadena, G. W. Crawford and H. A. W. Spetzler, *Radiat. Res.*, 1962, **17**, 11.
17 M. Z. Heydari, E. Malinen, E. O. Hole and E. Sagstuen, *J. Phys. Chem. A*, 2002, **106**, 8971.
18 D. F. Regulla and U. Deffner, *Int. J. Appl. Radiat. Isot.*, 1982, **33**, 1101.
19 A. Lund, S. Olsson, M. Bonora, E. Lund and H. Gustafsson, *Spectrochim. Acta, Part A*, 2002, **58**, 1301.
20 G. Budgell, J. Berresford, M. Trainer, E. Bradshaw, P. Sharpe and P. Williams, *Radiother. Oncol.*, 2011, **99**, 246.
21 D. McDonald, C. Yount, N. Koch, M. Ashenafi, J. Peng and K. Vanek, *Med. Phys.*, 2011, **38**, 1685.
22 E. Pantelis, A. Moutsatsos, K. Zourari, W. Kilby, C. Antypas, P. Papagiannis, P. Karaiskos, E. Georgiou and L. Sakelliou, *Med. Phys.*, 2010, **37**, 2369.
23 D. Wagner, M. Anton and H. Vorwerk, *Phys. Med. Biol.*, 2011, **56**, 1373.
24 O. A. Sauer and J. Wilbert, *Med. Phys.*, 2007, **34**, 1983.
25 F. Chen, C. F. O. Graeff and O. Baffa, *Appl. Radiat. Isot.*, 2005, **62**, 267.
26 F. C. Abrego, C. S. G. Calcina, A. de Almeida, C. E. de Almeida and O. Baffa, *Med. Phys.*, 2007, **34**, 1573.
27 F. Chen, C. F. O. Graeff and O. Baffa, *Nucl. Instrum. Methods Phys. Res., Sect. B*, 2007, **264**, 277.
28 A. Mack, S. G. Scheib, J. Major, S. Gianolini, G. Pazmandi, H. Feist, H. Czempiel and H. J. Kreiner, *Med. Phys.*, 2002, **29**, 2080.
29 F. Brai, G. Gennaro, M. Marrale, A. Bartolotta and M. C. D'Oca, *Appl. Radiat. Isot.*, 2007, **65**, 435.
30 F. Chen, J. V. Ramirez, P. Nicolucci and O. Baffa, *Health Phys.*, 2010, **98**, 383.
31 F. Chen, P. Nicolucci and O. Baffa, *Radiat. Meas.*, 2008, **43**, 467.
32 M. K. K. Leung, J. C. L. Chow, B. D. Chithrani, M. J. G. Lee, B. Oms and D. A. Jaffray, *Med. Phys.*, 2011, **38**, 624.
33 M. Marrale, A. Longo, M. Spanò, A. Bartolotta, M. C. D'Oca and M. Brai, *Radiat. Res.*, 2011, **175**, 6.
34 E. J. Guidelli, A. P. Ramos, M. E. D. Zaniquelli and O. Baffa, *Spectrochim. Acta, Part A*, 2011, **82**, 140.
35 C. Krishnaraj, E. G. Jagan, S. Rajasekar, P. Selvakumar, P. T. Kalaichelvan and N. Mohan, *Colloids Surf., B*, 2010, **76**, 50.
36 I. Medina-Ramirez, S. Bashir, Z. Luo and J. L. Liu, *Colloids Surf., B*, 2009, **73**, 185.
37 S. D. Solomon, M. Bahadory, A. V. Jeyarajasingam, S. A. Rutkowsky, C. Boritz and L. Mulfinger, *J. Chem. Educ.*, 2007, **84**, 322.
38 A. Rafey, K. B. L. Shrivastavaa, S. A. Iqbal and Z. Khan, *J. Colloid Interface Sci.*, 2011, **354**, 190.
39 Y. G. Sun and Y. N. Xia, *Science*, 2002, **298**, 2176.
40 A. Tomal, D. M. Cunha, M. Antoniassi and M. E. Poletti, *Appl. Radiat. Isot.*, 2012, DOI: 10.1016/j.apradiso.2011.11.044.
41 National Institute of Standards and Technology-NIST, *Physical Reference Data*, 2009.

42 N. G. Khlebtsov, *Quantum Electron.*, 2008, **38**, 504.

43 I. Medina-Ramirez, S. Bashir, Z. P. Luo and J. L. Liu, *Colloids Surf., B*, 2009, **73**, 185.

44 G. J. Lee, S. I. Shin, Y. C. Kim and S. G. Oh, *Mater. Chem. Phys.*, 2004, **84**, 197.

45 S. Link, M. A. El-Sayed and M. B. Mohamed, *J. Phys. Chem. B*, 2005, **109**, 10531.

46 T. Saraidarov, V. Levchenko, I. Popov and R. Reisfeld, *Superlattices Microstruct.*, 2009, **46**, 171.

47 T. Araki and H. Tanaka, *Phys. Rev. E: Stat., Nonlinear, Soft Matter Phys.*, 2006, **73**, 061506-1.

48 A. C. Balazs, T. Emrick and T. P. Russell, *Science*, 2006, **314**, 1107.

49 Q. Chen, L. Yue, F. Xie, M. Zhou, Y. Fu, Y. Zhang and J. Weng, *J. Phys. Chem. C*, 2008, **112**, 10004.

50 Q. Shen, J. Sun, H. Wei, Y. Zhou, Y. Su and D. Wang, *J. Phys. Chem. C*, 2007, **111**, 13673.

51 Y. R. Ma, H. Colfen and M. Antonietti, *J. Phys. Chem. B*, 2006, **110**, 10822.

52 D. Schwahn, Y. R. Ma and H. Colfen, *J. Phys. Chem. C*, 2007, **111**, 3224.

53 M. Niederberger and H. Colfen, *Phys. Chem. Chem. Phys.*, 2006, **8**, 3271.

54 B.-q. Shentu, J.-p. Li and Z.-x. Weng, *Chin. J. Polym. Sci.*, 2007, **25**, 227.

55 D. Garcia-Lopez, J. C. Merino and J. M. Pastor, *J. Appl. Polym. Sci.*, 2003, **88**, 947.

56 M. Koyama, M. Shiraishi, K. Sasaki and K. Kon-no, *J. Dispersion Sci. Technol.*, 2008, **29**, 1266.

57 R. B. Thompson, V. V. Ginzburg, M. W. Matsen and A. C. Balazs, *Science*, 2001, **292**, 2469.

58 J. U. Kim and B. O'Shaughnessy, *Macromolecules*, 2006, **39**, 413.

59 D. Jaikumar, S. Kalainathan and G. Bhagavanarayana, *J. Cryst. Growth*, 2009, **312**, 120.

60 M. L. Caroline, R. Sankar, R. M. Indirani and S. Vasudevan, *Mater. Chem. Phys.*, 2009, **114**, 490.

61 M. B. Tarallo, A. J. Costa-Filho, E. D. Vieira, A. Monge, C. Q. Leite, G. Borthagaray, D. Gambino and M. H. Torre, *An. Asoc. Quim. Argent.*, 2009, **97**, 9.

62 A. M. Alabanza and K. Aslan, *Cryst. Growth Des.*, 2011, **11**, 4300.

63 N. A. Kotov, M. E. D. Zaniquelli, F. C. Meldrum and J. H. Fendler, *Langmuir*, 1993, **9**, 3710.

64 J. Y. Lee, Q. L. Zhang, T. Emrick and A. J. Crosby, *Macromolecules*, 2006, **39**, 7392.

65 B. J. Kim, J. Bang, C. J. Hawker and E. J. Kramer, *Macromolecules*, 2006, **39**, 4108.

66 S. Gupta, Q. L. Zhang, T. Emrick, A. C. Balazs and T. P. Russell, *Nat. Mater.*, 2006, **5**, 229.

67 E. Malinen, E. A. Hult, E. O. Hole and E. Sagstuen, *Radiat. Res.*, 2003, **159**, 149.